DOI: 10.1002/asia.200600194

Metallodielectric Hollow Shells: Optical and Catalytic Properties

Isabel Pastoriza-Santos,* Jorge Pérez-Juste,* Susana Carregal-Romero, Pablo Hervés, and Luis M. Liz-Marzán[a]

Abstract: Metallodielectric composites with tunable optical properties were prepared by layer-by-layer assembly of gold nanorods on polystyrene (PS) spheres and subsequent deposition of SiO_2 or TiO_2 encapsulating shells through a sol–gel process. The optical properties of the core-shells were tailored in the visible and the near-infrared region through the gold nanorod aspect ratio and the gold nanoparticle density. Removal of the PS core by dissolution in an appropriate solvent, such as THF, yielded metallodielectric hollow shells with optical properties identical to those of the original composites. The presence of gold and the porosity of the SiO_2 or TiO_2 shells, suitable to allow diffusion of reactants and products, make these materials of interest as catalysts, as demonstrated by the reduction of potassium hexacyanoferrate(III) with $NaBH_4$.

Keywords: gold · heterogeneous catalysis · nanostructures · hollow shell structures · sol–gel processes

Introduction

Research on (organic or inorganic) hollow shells has advanced dramatically during the last few years because a large number of applications have been identified and predicted in different fields such as pharmaceuticals, medicine, materials science, and catalysis.[1–3] A specific feature of hollow shells is their relatively low density, which generally makes them more attractive than the corresponding core-shell particles. Although some template-free approaches can be found in the literature for the fabrication of shells,[4–9] to date, template-mediated methods have been most popular and still provide better control of the final morphology. One of the first and most widely used template-mediated methods relies on the well-known layer-by-layer (LBL) assembly technique[10] and comprises the stepwise deposition onto a colloidal template of polyelectrolytes and other materials (such as nanoparticles) driven by electrostatic interactions to form core-shell composites and the subsequent removal of the core with a solvent (dissolution)[11] or by heating (calcination).[12] The main advantage of this approach is its enormous versatility, as the composition can be easily tuned by simple combination of the polyelectrolytes with appropriate materials (polymers, nanoparticles, etc.), thus providing control over the mechanical, optical, and surface properties, among others. The presence of silica in the layered structure is known to improve the mechanical properties and to provide control over the permeability of the polyelectrolyte-based nanocapsules.[12,13] On the other hand, the combination of a diazoresin, acting as polycation, with polyelectrolytes has been used to enhance resistance toward etching by solvents.[14] Recently, hollow colloids with novel optical properties were obtained by the LBL-based assembly of metal nanoparticles on spherical templates.[15,16] Polyelectrolyte multilayer capsules doped with metal nanoparticles are also interesting for biomedical applications, as these can act as radiation-absorbing centers for the remote release of encapsulated materials[17–20] or as delivery vehicles and supports in biosensing.[21] Catalytic applications have also been envisaged, because metal nanoparticles are efficient catalysts[22,23] and the hollow capsules present large surface areas.[24] Another advantage of this approach is the possibility to build multifunctional capsules with different properties, as was recently demonstrated with the incorporation of magnetic and luminescent properties by simultaneous doping with CdTe nanocrystals and Fe_3O_4 nanoparticles[25] or of magnetic and antimicrobial properties through combination of goethite with silver nanoparticles.[26]

[a] Dr. I. Pastoriza-Santos, Dr. J. Pérez-Juste, S. Carregal-Romero, Dr. P. Hervés, Prof. L. M. Liz-Marzán
Departamento de Química Física and Unidad Asociada CSIC
Universidade de Vigo
36310 Vigo (Spain)
Fax: (+34) 986-812-556
E-mail: pastoriza@uvigo.es

Supporting information for this article is available on the WWW under http://www.chemasianj.org or from the author.

Another particularly interesting template-mediated method to fabricate hollow capsules is based on the direct precipitation of inorganic molecule precursors[27–30] onto the template, which may have been previously functionalized with specific groups to enhance the coating.[31–33] As in the previous method, the template is subsequently removed by dissolution or calcination. This method is particularly useful to obtain hollow spheres of ceramic materials such as silica, titania, or yttria.

Herein we present a synthetic procedure for the fabrication of metallodielectric hollow shells comprising a composite made of gold nanorods within a metal oxide matrix, such as silica or titania. The procedure combines the LBL method for controlled deposition of gold rods on polystyrene spheres and a sol–gel process for producing a silica or titania outer shell. We demonstrate that the gold nanoparticles can provide the capsules with optical tunability simply by changing the nanorod morphology (aspect ratio) or by adjusting their density. Additionally, the catalytic activity of such composite colloids is demonstrated by using the reduction of potassium hexacyanoferrate(III) with $NaBH_4$ as a test reaction.

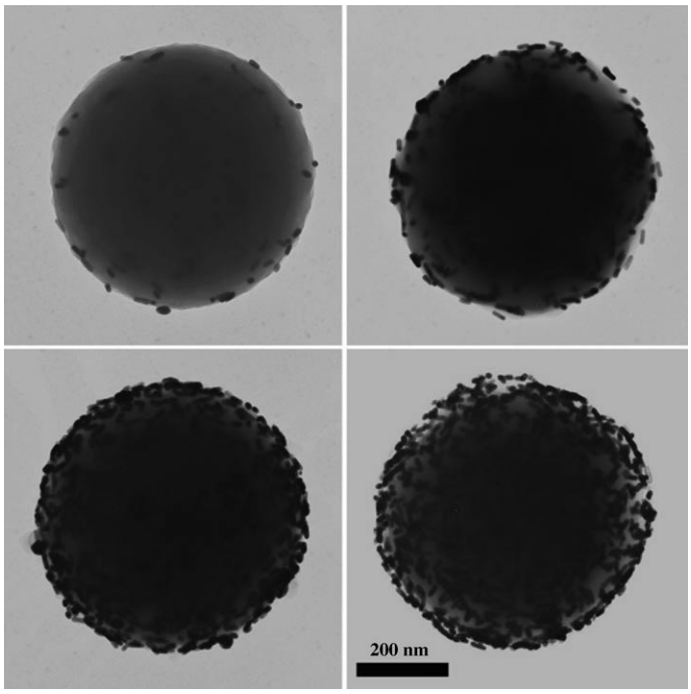

Figure 1. TEM micrographs of polystyrene microspheres coated with increasing gold nanorod density. The Au nanorods have an aspect ratio of 3.1.

Results and Discussion

Formation of Hollow Ceramic Microspheres Doped with Gold Nanorods

One of the main targets of this work was the synthesis of hollow microcapsules with optical and catalytic functionalities through homogeneous doping with gold nanorods. The optical response in the visible and near-infrared (NIR) region can be modulated either by tuning the gold nanorod aspect ratio or by controlling the gold nanorod concentration within the microcapsules. Although several works on noble-metal-nanoparticle-doped hollow or core-shell microspheres have been reported,[4,15–18,25,26,34] most of them do not focus on the study of the optical properties, and for this reason metal nanoparticles are sometimes prepared by chemical reduction in situ (allowing poor control of the final nanoparticle morphology and therefore of the resulting optical properties), rather than by using preformed metal nanoparticles to obtain the nanocomposites. Our choice was a multistep process involving the initial synthesis of the metal nanoparticles followed by deposition onto colloidal templates, prior to shell formation, as this allows far better control over the ultimate optical properties of the composite. Additionally, the density of gold nanoparticles can be varied by simply changing the amount of nanoparticles during the process (Figure 1).

The sacrificial templates used to obtain the metal-doped capsules were polystyrene (PS) beads, 705 nm in diameter with a surface charge of approximately −33 mV, whereas the metal nanoparticles were gold nanorods (aspect ratio 3.1 and 4.8)[35] stabilized with poly-*N*-vinylpyrrolidone (PVP) and thus with a negative surface charge (zeta potential = −20 mV). Gold nanorod deposition on the PS beads was carried out through polyelectrolyte-driven LBL assembly,[10,11] which required prior assembly of a polyelectrolyte multilayer film (PDDA/PSS/PDDA) on the PS spheres so as to obtain uniform, positively charged surfaces onto which the negatively charged gold rods would readily stick. Multiple nanorod additions (11 additions, 10-min intervals) yielded a uniform, random assembly of the metal nanoparticles on the modified PS surface, as can be seen in Figure 1 for rods with aspect ratio of 3.1 (experiments in which nanorods with aspect ratio 4.8 were used showed the same trend; see Supporting Information).

Although hollow capsules can be made of layered polyelectrolytes,[11] coating with SiO_2 has been shown to provide hollow capsules with improved long-term storability, robustness, mechanical strength, and controllable permeability.[13] In the work reported herein, silica coating was carried out on the nanorod-decorated PS spheres by using the Stöber process after coating with an extra PVP layer to enhance the surface affinity toward silica.[36] This procedure allowed the thickness of the silica layer to be tuned by varying the amount of tetraethoxysilane (TEOS), as shown in Figure 2a and b. Notably, after silica coating, deformation of some core-shell particles was observed (see Supporting Information). This effect is induced by ammonia, which is able to dissolve the PS templates during the formation of the silica shell, and therefore if TEOS hydrolysis and condensation is not fast enough to form a protecting silica shell, the diffusion out of the shell of the PS congregates can induce the deformation or even the rupture of the core-shell composites.[37] A similar procedure, based on the hydrolysis of a ti-

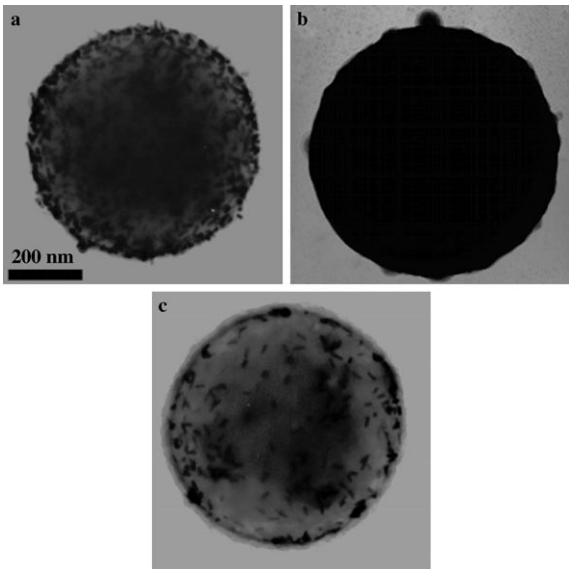

Figure 2. a), b) TEM micrographs of Au-rod-doped PS microspheres coated with 4- and 25-nm-thick silica shells, respectively. c) TEM micrograph of Au-rod-doped PS microsphere coated with a 12-nm-thick titania shell. In a) and b), maximum gold nanoparticle density can be seen, whereas in c) only 35% of maximum gold density was achieved.

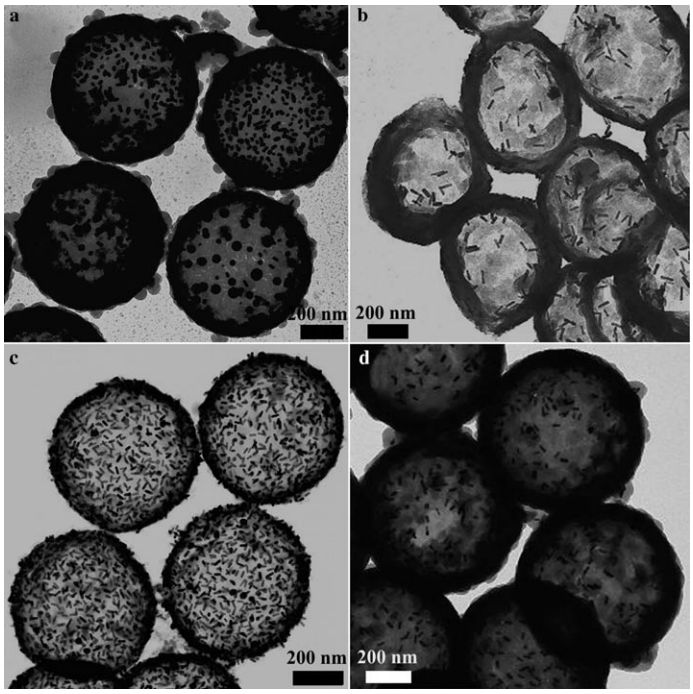

Figure 3. TEM micrographs of a) Au/SiO_2 capsules obtained by calcination at 400 °C, b) Au/TiO_2, and c), d) Au/SiO_2 capsules obtained by dissolution with THF (see text for further details). In a) and c), the PS beads were loaded with maximum gold density, whereas in b) and d) the loading is 35% of the maximum density.

tanium alkoxide, can be used to coat the Au-modified PS spheres with TiO_2 (Figure 2c),[27] which is expected to enhance the versatility of this system, as the dielectric properties of titania, which is a wide-bandgap semiconductor, are more interesting than those of silica for a number of applications.[38–43]

Upon the growth of ceramic shells, PS cores can be removed to obtain hollow Au/SiO_2 or Au/TiO_2 composite capsules, which are much more lightweight materials. The core can be removed either through dissolution with a suitable solvent[11] or through calcination,[12] which was found to be more convenient in previous works, in particular for thick silica shells. However, in the present study calcination (300–400 °C) would lead to drastic optical changes because of the thermal reshaping of the gold nanorods into spheres, as previously reported[44] and confirmed in Figure 3a. For this reason, Au/SiO_2 and Au/TiO_2 hollow capsules were obtained by core dissolution using with tetrahydrofuran (e.g. Figure 3b–d). It should be noted that for the growth of thicker Au/SiO_2 capsules (Figure 3d) it was more efficient to prepare thin capsules and then carry out further growth, as dissolution through thicker shells is hindered.

Optical and Catalytic Properties of the Nanocomposites

An analysis of the optical properties of the composites is presented on the basis of the dielectric environment around the rods and possible interparticle interactions. In Figure 4, the evolution of UV/Vis/NIR spectra is shown for PS microspheres coated with two different gold nanorod samples (aspect ratio 3.1 (a) and 4.8 (b)), in which the density of gold nanorods is increased by successive additions. It can be seen that the longitudinal plasmon band of the gold–PS nanocomposites (position and width, see insets) changes when the surface density of the gold nanorods on the PS surface gradually increases. This is related to increased dipole coupling among neighboring gold nanoparticles as the separation between nanoparticles decreases, which has been shown to be responsible for red shifting and broadening of plasmon resonance bands.[45] Remarkably, for the same number of additions, a much larger red shift (68 nm) was observed for "long" nanorods (aspect ratio 4.8) than for "short" rods (aspect ratio 3.1; 35-nm shift). Considering that both gold nanorod samples have roughly the same gold concentration, for the longer rods a lower number of particles is expected on the PS beads (which was confirmed with SEM, see Figure 5). Nevertheless, dipole coupling seems to be stronger, which is presumably related to the relationship between interparticle separation and nanoparticle dimensions, which is still smaller for the longer rods, thus leading to stronger coupling.

Upon coating of the nanorod-modified PS particles with silica or titania, dipole–dipole interactions are expected to be screened because of an insulating effect of the metal oxides. For this reason, even though the refractive index of silica is larger than that of water or ethanol, it was found that the deposition of an outer silica shell leads to a blue shift (Figure 6). It was previously demonstrated[45] that when metallic nanoparticles are surrounded by an insulating material such as silica, an electron-tunnelling barrier can be cre-

CHEMISTRY
AN ASIAN JOURNAL

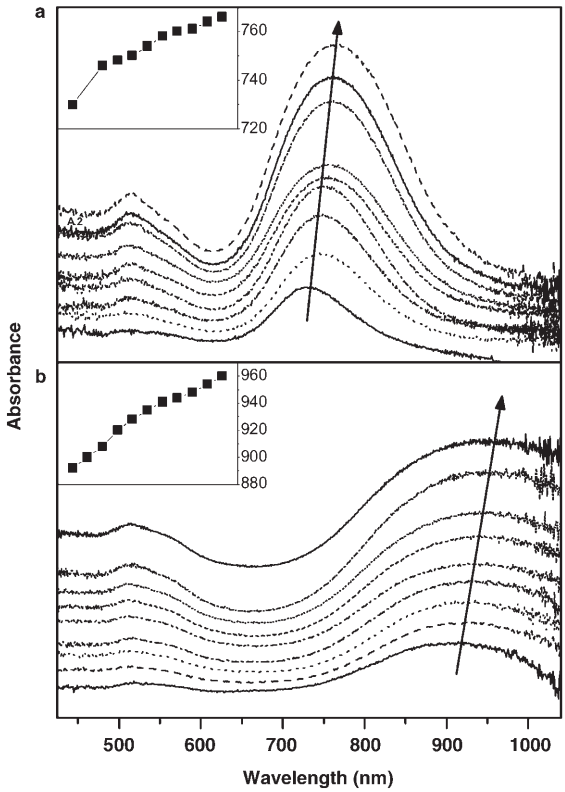

Figure 4. UV/Vis spectra of gold nanorod/PS microsphere composites with varying nanorod density; a) and b) correspond to experiments carried out with gold nanorods of aspect ratios 3.1 and 4.8, respectively. The insets are plots of the position of the longitudinal plasmon band versus the number of gold-rod additions.

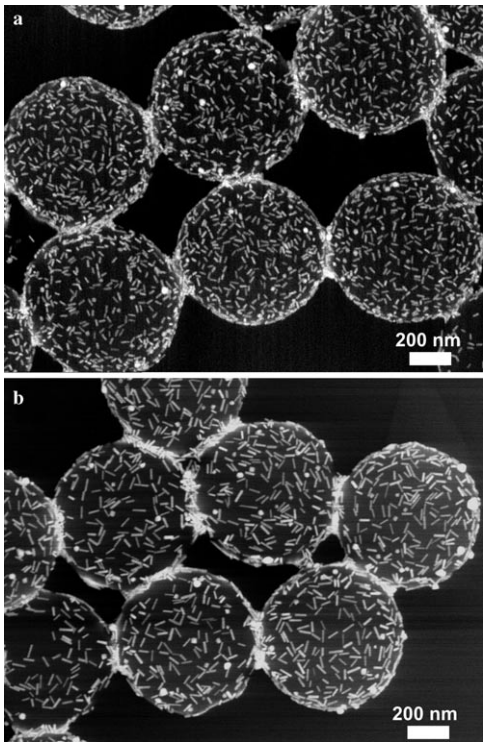

Figure 5. SEM images (YAG detector) of PS microspheres coated with the same gold density, but using nanorods with different aspect ratios: a) 3.1, b) 4.8.

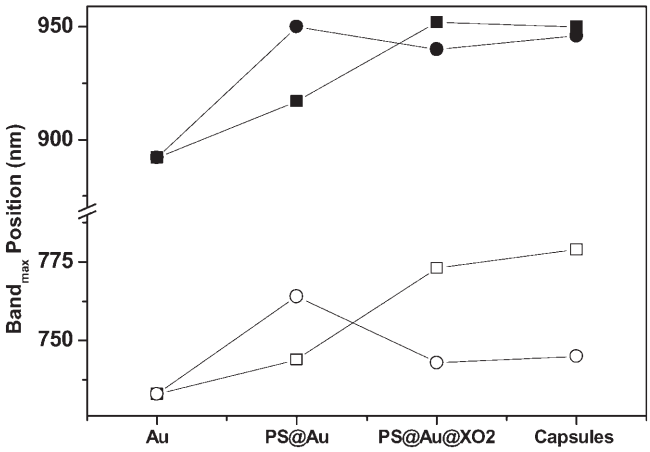

Figure 6. Maximum wavelength of the longitudinal plasmon band for different samples: Au nanorods, Au nanorod assembled on PS spheres, PS coated with Au/SiO_2 (circles), or Au/TiO_2 (squares), and the corresponding capsules formed upon dissolution of the PS core. Data are shown for rods with average aspect ratio 3.1 (open symbols) and 4.8 (solid symbols).

ated between the metal nanoparticles, thereby (partially) screening the dipole coupling between neighboring particles.

When the gold-rod-decorated PS microspheres are coated with TiO_2, which has a much higher refractive index (2.4 versus 1.46 for silica), an additional red shift is observed, meaning that the refractive index effect clearly overcomes the screening effect, which on the other hand may be lower if we take into account the semiconductor character of titania.

Finally, although the dissolution of the PS cores and the formation of hollow shells lead to a decrease in the scattering contribution (data not shown), it does not affect the position of the longitudinal plasmon band, so that the optical properties of the capsules are identical to those of the core-shells. The reason for this is that the rods are essentially embedded within the ceramic shells and are not affected by any changes in the outer environment.

These particles are not only interesting because of their optical properties, but can also be used as efficient catalysts as silica or titania shells have been shown to be sufficiently porous to allow diffusion of reactants and products.[29,46] We demonstrated this efficiency through analysis of the effect of Au–SiO_2 hollow shells on the kinetics of the reduction of potassium hexacyanoferrate(III) with $NaBH_4$ which can be considered as a model electron-transfer reaction.[47] In the absence of metal nanoparticles, this reaction was previously reported to behave as a zero-order reaction in hexacyanoferrate(III),[48] with an activation energy of 30 kJ mol^{-1}, whereas in the presence of colloidal gold the reaction mechanism becomes first order and the activation energy of the catalyzed reaction was found to be almost ten times lower (4 kJ mol^{-1}).[47] The catalysis mechanism seems

to involve rapid cathodic polarization of the metallic nanoparticles by sodium borohydride [Eq. (1)], followed by transfer of excess surface electrons to ferricyanide ions reaching the particles, which are then reduced in what would then become the slow step of the reaction [Eq. (2)].

$$BH_4^- + Au \rightleftharpoons Q^- \quad \text{(fast)} \tag{1}$$

$$Q^- + [Fe(CN)_6]^{3-} \rightarrow [Fe(CN)_6]^{4-} + Q \quad \text{(slow)} \tag{2}$$

In all runs, the concentration of $NaBH_4$ was chosen to exceed the concentration of hexacyanoferrate(III). In this way, the kinetics of the reduction process can be treated as a pseudo-first-order reaction in hexacyanoferrate. The progress of the reduction was monitored through changes in the UV/Vis spectra, as shown in Figure 7a for gold nanorod/silica hollow spheres (see TEM image in Figure 7b). The characteristic absorption peak of hexacyanoferrate(III) at 420 nm decreases with time (as it is reduced to ferrocyanide), whereas the gold rod plasmon bands (around 520 and 900 nm for the transverse and longitudinal bands, respectively) are unaffected, which shows that the electron-transfer reaction proceeds through the pores of amorphous silica, but the morphology and distribution of the rods remain intact during the process.

An example of the excellent agreement of the experimental data with first-order kinetics is shown in the inset of Figure 7a for two different particle concentrations, using the corresponding integrated kinetic Equation (3):

$$\ln\left(\frac{A_t - A_\infty}{A_0 - A_\infty}\right) = -k_{obs}t \tag{3}$$

An increase in the concentration of the capsules by a factor of two produces a 2.9-fold increase in the observed rate constant (from 8.63×10^{-3} to $0.025\ s^{-1}$).

A similar catalytic effect was observed with gold-doped titania hollow shells. Figure 8a shows a representative spec-

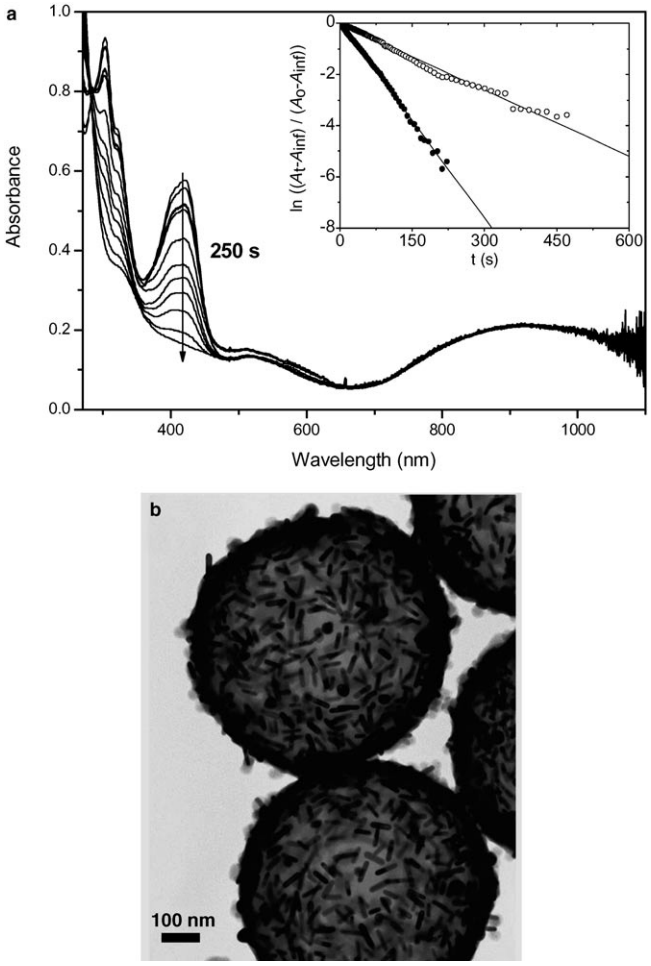

Figure 7. a) Spectral evolution of a mixture of hexacyanoferrate(III) and Au/SiO_2 metallodielectric capsules upon addition of sodium borohydride. $[[Fe(CN)_6]^{3-}]=8.33\times10^{-4}$ M, $[BH_4^-]=8.33\times10^{-3}$ M. The inset shows the linearized data for first-order analysis according to Equation (3) for two different capsule concentrations (see text for details). b) Representative TEM image of the Au/SiO_2 capsules used in this study.

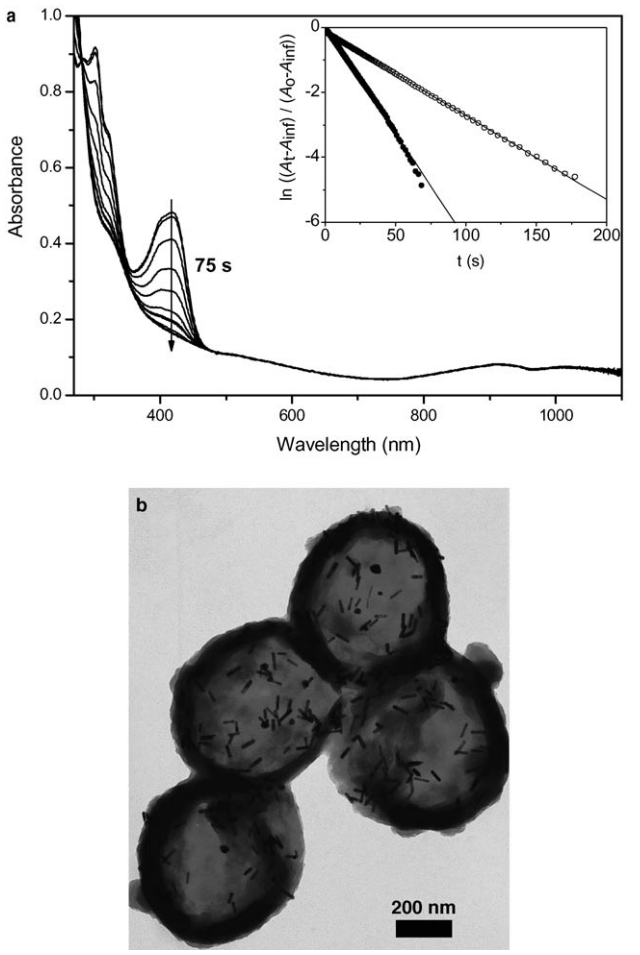

Figure 8. a) Spectral evolution of a mixture of hexacyanoferrate and Au/TiO_2 metallodielectric composites upon addition of sodium borohydride $[[Fe(CN)_6]^{3-}]=8.33\times10^{-4}$ M, $[BH_4^-]=8.33\times10^{-3}$ M. The inset shows the linearized data for first-order analysis according to Equation (3) for two different concentrations (see text for details). b) TEM image of the Au/TiO_2 capsules used in this study.

tral evolution of the reaction. As in the case of the silica shells, an increase in the amount of the titania capsules by a factor of almost two produces an increase in the pseudo-first-order of the reaction by a factor of 2.6 (from 0.024 up to 0.063 s^{-1}). Interestingly, although the amount of particles per capsule is lower (35% of the maximum gold density) in the case of the titania shells (relative to 100% for silica shells), as can be deduced from the intensity of the longitudinal plasmon band located around 925 nm (0.21 versus 0.08) and confirmed by TEM (see Figures 7b and 8b), kinetic experiments were consistently faster when using titania shells (0.063 s^{-1} vs. 0.025 s^{-1}). Therefore, gold-doped titania shells seem to display a higher catalytic efficiency than that of the analogous silica shells, but further evidence is needed to understand this result, and experiments in this direction are currently underway.

The advantage of using these composite particles, rather than free gold nanoparticles lies on the stability toward factors such as ionic strength or solvent exchange provided by the outer silica shell, or the easy removal (by centrifugation) upon completion of the catalytic process. It should be also pointed out that the pore size as well as the thickness of the silica shell should play an important role in modulating the catalytic properties of these composites, which is currently under investigation and will be reported elsewhere.

Conclusions

Metallodielectric hollow shells with tunable optical properties can be easily obtained by a three-step process consisting of a) LBL assembly of gold nanorods, b) deposition of SiO_2 or TiO_2 through a sol–gel process, and c) removal of the PS core by dissolution with an appropriate solvent. The optical properties of the hollow shells are due to the presence of gold nanoparticles, hence they can be tuned in the visible and the NIR regions by simply varying the gold nanorod aspect ratio or by controlling the nanoparticle density. Although the ceramic layer can provide mechanical stability, their porosity allows the use of the metallodielectric shells as catalysts for the reduction of potassium hexacyanoferrate-(III) with $NaBH_4$.

Experimental Section

Materials

Polystyrene beads (diameter 705 nm) were purchased from Ikerlat Polymers (Spain). Tetrachloroauric acid ($HAuCl_4 \cdot 3H_2O$), sodium borohydride, ascorbic acid, sodium chloride (NaCl), HCl, NH_4OH (32%), cetyltrimethyl ammonium bromide (CTAB), tetraethylorthosilicate (TEOS), and tetrahydrofuran (THF) were purchased from Aldrich. PVP (MW = 10000, 40000, and 360000) and tetraisopropyl orthotitanate (TTIP) were supplied by Fluka. Poly(styrenesulfonate) (PSS, MW = 70000), poly(diallyldimethylammonium chloride) (PDDA, MW = 200000–350000, 20 wt%) was procured from Sigma. Potassium hexacyanoferrate(III) was purchased from Scharlab. All chemicals were used as received. Pure grade ethanol and Milli-Q grade water were used to make up all solutions.

Particle Synthesis

Gold nanorods were synthesized according to the protocols proposed by Nikoobakht et al.[49] and Liu et al.[50] First, a gold seed solution was prepared by reduction of $HAuCl_4$ (0.25 mM, 5 mL) with sodium borohydride (0.01 M, 0.3 mL) in an aqueous surfactant solution of CTAB (0.1 M). The average particle size measured from TEM was 2.8 ± 0.7 nm. For the synthesis of gold nanorods with aspect ratio 3.1, seed solution (60 μL) was added to a growth solution containing CTAB (0.1 M), $HAuCl_4$ (0.5 mM), ascorbic acid (0.75 mM), and silver nitrate (0.075 mM). For the synthesis of gold nanorods with aspect ratio 4.8, seed solution (24 μL) was added to a growth solution containing CTAB (0.1 M), $HAuCl_4$ (0.5 mM), ascorbic acid (0.8 mM), HCl (0.019 M), and silver nitrate (0.12 mM). After the excess CTAB was removed by centrifugation (8500 rpm), the particles were transferred into ethanol for surface functionalization with PVP (MW = 40000).[51] Sufficient PVP to coat the particles with 60 monomers per nm^2 of surface area was added to the gold nanorods. The mixture was stirred overnight, excess PVP was removed by centrifugation, and the particles were redispersed in ethanol.

Polyelectrolyte Coating

Positively charged PDDA (1 mg mL^{-1} in water containing NaCl (0.5 M); 1.8 mL) was added to an aqueous suspension of negatively charged PS particles (10 wt%; 0.1 mL) with a diameter of 705 nm. After 15 min (to allow the polyelectrolytes to adsorb onto the PS nanoparticle surface), the non-adsorbed polyelectrolyte was removed by three cycles of centrifugation (6000 rpm for 5 min), and the particles were redispersed in water. In the last cycle, the particles were redispersed in water (0.1 mL). The negatively charged PSS was then subsequently adsorbed onto the particles by adding PSS (1 mg mL^{-1} in water containing NaCl (0.5 M); 1.8 mL) to the PDDA-coated PS suspension, allowing 20 min for PSS adsorption, and removing excess PSS by three cycles of centrifugation. The particles were resdispersed in water. An additional layer of PDDA was deposited by using the same conditions and procedure.

Gold Coating

The PVP-coated gold nanorods were deposited onto the polyelectrolyte-coated PS particles in a multistep process. In each step, a solution of Au nanoparticles in ethanol (6.63 mM in gold; 2 mL) was added to PS beads (1 mg) dispersed in ethanol (1 mL) under sonication. The mixture was stirred for 10 min to allow equilibration. Prior to each addition of gold nanoparticles a cycle of centrifugation and redispersion in ethanol was carried out to remove the non-adsorbed gold particles.

Silica Coating

The gold coated PS particles (1 mg of the polyelectrolyte-coated spheres) were redispersed in ethanol (2 mL). A solution of ammonia in ethanol (containing 300 μL of concentrated aqueous ammonia (33 wt%); 1.2 mL) was added under stirring, and then a solution of TEOS in ethanol (2.0 vol%; 0.10 mL) was added under gentle stirring. The mixture was allowed to react for 6 h. At this point the beads present a 4-nm thick silica shell. Further additions of TEOS were carried out to allow growth of the silica shells.

Titania Coating

An aqueous solution of NaCl (5 mM; 32 μL) was added to ethanol (1.34 mL) containing PVP (MW = 360000; 13.5 mg). Ethanol (0.1 mL) containing the gold-coated PS particles (1 mg of the polyelectrolytes-coated particles) was added dropwise. Finally, TTIP (14.5 μL) in ethanol (0.193 mL) was added under vigorous stirring. After 1 min, stirring was stopped, and the suspension was allowed to stand for 15 min. The particles were centrifuged and redispersed in ethanol to remove any residual small titania nanoparticles as well as PVP, which is no longer necessary for stabilization.

Hollow Spheres

The hollow capsules were prepared by either calcination (at 450°C for 1 h) or by treatment with THF, that is, exposure of the silica- or titania-

coated PS particles (1 mg) to THF (4 mL) for 24 h. After this treatment the hollow spheres were centrifuged at 6000 rpm for 10 min and redispersed in ethanol. Exposure to THF was repeated twice to ensure the complete core removal.

Characterization

A JEOL JEM 1010 transmission electron microscope operating at an acceleration voltage of 100 kV was used for low-magnification imaging. SEM characterization was carried out with a JEOL JSM-6700F FEG-SEM operating at an acceleration voltage of 10 kV in backscattering-electron image (YAG). UV/Vis/NIR spectra were measured with a Cary 5000 UV-Vis-NIR spectrophotometer. The zeta potential was determined by electrophoretic mobility measurements with a Malvern Zetasizer 2000 instrument.

Kinetic Measurements

The reactions were carried out at room temperature in a diode-array UV/Vis spectrophotometer Agilent 8453. All solutions were previously deaerated, and the reaction mixtures were maintained at pH 11.5 to avoid decomposition of $NaBH_4$.[52] Kinetic data were always satisfactorily fitted by the first-order integrated rate equations in hexacyanoferrate concentration. Experiments were reproducible to within 5%.

Acknowledgements

This work was supported by the Spanish Ministerio de Educación y Ciencia/FEDER (Projects NAN2004-09133 and MAT2004-02991). S.C.-R. is grateful for an FPI research grant. The authors thank J. Pérez-Borrajo and J. B. Rodríguez-González for their assistance with SEM measurements.

[1] F. Caruso, *Chem. Eur. J.* **2000**, *6*, 413.
[2] F. Caruso, *Adv. Mater.* **2001**, *13*, 11.
[3] *Hollow and Solid Spheres and Microspheres: Science and Technology Associated with their Fabrication and Application*, *Vol. 372* (Eds.: D. L. Wilcox, Sr., M. Berg, T. Bernat, D. Kellerman, J. K. Cochran, Jr.), Materials Research Society, Pittsburgh, PA, **1995**.
[4] X. Cao, L. Gu, L. Zhuge, W. Gao, W. Wang, S. Wu, *Adv. Funct. Mater.* **2006**, *16*, 896.
[5] Y. Yin, R. M. Rioux, K. C. Erdonmez, S. Hughes, G. A. Somorjai, A. P. Alivisatos, *Science* **2004**, *304*, 711.
[6] Y. Sun, Y. Xia, *Science* **2002**, *298*, 2176.
[7] Y. Sun, B. Mayers, Y. Xia, *Adv. Mater.* **2003**, *15*, 641.
[8] J. X. Huang, Y. Xie, B. Li, Y. Liu, Y. T. Quian, S. Y. Zhang, *Adv. Mater.* **2000**, *12*, 808.
[9] M. Jujiwara, K. Shiokawa, Y. Tanaka, Y. Nakahara, *Chem. Mater.* **2004**, *16*, 5420.
[10] G. Decher, *Science* **1997**, *277*, 1232.
[11] E. Donath, G. B. Sukhorukov, F. Caruso, S. A. Davies, H. Möhwald, *Angew. Chem.* **1998**. *110*, 2323; *Angew. Chem. Int. Ed.* **1998**. *37*, 2201.
[12] F. Caruso, R. A. Caruso, H. Möhwald, *Science* **1998**, *282*, 1111.
[13] B. Sun, S. A. Mutch, R. M. Lorenz, D. T. Chiu, *Langmuir*, **2005**, *21*, 10763.
[14] I. Pastoriza-Santos, B. Schöler, F. Caruso, *Adv. Funct. Mater.* **2001**, *11*, 122.
[15] F. Caruso, M. Spasova, V. Salgueiriño-Maceira, L. M. Liz-Marzán, *Adv. Mater.* **2001**, *13*, 1090.
[16] T. Cassagneau, F. Caruso, *Adv. Mater.* **2002**, *14*. 732.
[17] A. G. Skirtach, C. Dejugnat, D. Braun, A. S. Susha, A. L. Rogach, W. J. Parak, H. Möhwald, G. Sukhorukov, *Nano Lett.* **2005**, *5*, 1371.
[18] A. G. Skirtach, A. A. Antipov, D. G. Shchukin, G. Sukhorukov, *Langmuir* **2004**, *20*, 6988.
[19] B. Radt, T. Smith, F. Caruso, *Adv. Mater.* **2004**, *16*, 2184.
[20] A. S. Angelatos, B. Radt, F. Caruso, *J. Phys. Chem. B* **2005**, *109*, 3071.
[21] F. Caruso, M. Spasova, A. Susha, M. Giersig, R. A. Caruso, *Chem. Mater.* **2001**, *13*, 109.
[22] Ch. Mohr, P. Claus, *Sci. Prog.* **2001**, *84*, 311.
[23] M. Haruta, *Catal. Today* **1997**, *36*, 1997.
[24] A. A. Antipov, G. Sukhorukov, Y. A. Fedutik, J. Hartmann, M. Giersig, H. Möhwald, *Langmuir* **2002**, *18*, 6687.
[25] B. Zebli, A. S. Susha, G. Sukhorukov, A. L. Rogach, W. J. Parak, *Langmuir* **2005**, *21*, 4262.
[26] W. S. Choi, H. Y. Koo, J.-H. Park, D.-Y.; Kim, *J. Am. Chem. Soc.* **2005**, *127*, 16136.
[27] A. Imhof, *Langmuir* **2001**, *17*, 3579.
[28] Y. Hotta, P. C. A. Alberius, L. Bergström, *J. Mater. Chem.* **2003**, *13*, 496.
[29] I. Pastoriza-Santos, D. S. Koktysh, A. A. Mamedov, M. Giersig, N. A. Kotov, L. M. Liz-Marzán, *Langmuir* **2000**, *16*, 2731.
[30] N. Kawahashi, E. Matijevic, *J. Colloid Interface Sci.* **1990**, *138*, 534.
[31] I. Tissot, J. P. Reymond, F. Lefebvre, E. Bourgeat-Lami, *Chem. Mater.* **2002**, *14*, 1325.
[32] Y. Chen, E.-T. Kang, K.-G. Neoh, A. Greiner, *Adv. Funct. Mater.* **2005**, *15*, 113.
[33] M. Giersig, T. Ung, L. M. Liz-Marzán, P. Mulvaney, *Adv. Mater.* **1997**, *9*, 570.
[34] Y. Yin, Y. Lu, B. Gates, Y. Xia, *Chem. Mater.* **2001**, *13*, 1146.
[35] The average lengths and diameters measured by TEM were 36.24 ± 3.01 and 11.66 ± 1.04 for rods with aspect ratio 3.1, and 54.97 ± 7.19 and 11.65 ± 1.72 for rods with aspect ratio 4.8.
[36] C. Graf, D. L. J. Vossen, A. Imhof, A. van Blaaderen, *Langmuir* **2003**, *19*, 6693.
[37] M. Chen, L. Wu, S. Zhou, B. You, *Adv. Mater.* **2006**, *18*, 801.
[38] B. O'Regan, M. Gratzel, *Nature* **1991**, *353*, 737.
[39] M. Wagemaker, A. P. M. Kentgens, F. M. Mulder, *Nature* **2002**, *418*, 397.
[40] R. Asahi, T. Morikawa, T. Ohwaki, K. Aoki, Y. Taga, *Science* **2001**, *293*, 269.
[41] W. Zhao, W. H. Ma, C. H. Chen, J. C. Zhao, Z. G. Shuai, *J. Am. Chem. Soc.* **2004**, *126*, 4782.
[42] R. Wang, K. Hashimoto, A. Fujishima, M. Chikuni, E. Kojima, A. Kitamura, M. Shimohigoshi, T. Watanabe, *Nature* **1997**, *388*, 431.
[43] D. L. Li, H. S. Zhou, I. Honma, *Nat. Mater.* **2004**, *3*, 65.
[44] H. Petrova, J. Pérez-Juste, I. Pastoriza-Santos, G. V. Hartland, L. M. Liz-Marzán, P. Mulvaney, *Phys. Chem. Chem. Phys.* **2006**, *8*, 814.
[45] L. M. Liz-Marzán, P. Mulvaney, *J. Phys. Chem. B* **2003**, *107*, 7312.
[46] T. Ung, L. M. Liz-Marzán, P. Mulvaney, *Langmuir* **1998**, *14*, 3740.
[47] S. Carregal-Romero, J. Pérez-Juste, P. Hervés, L. M. Liz-Marzán, unpublished results.
[48] T. Freund, *J. Inorg. Nucl. Chem.* **1959**, *9*, 246.
[49] B. Nikoobakht, M. A. El-Sayed, *Chem. Mater.* **2003**, *15*, 1957.
[50] M. Liu, P. Guyot-Sionnest, *J. Phys. Chem. B* **2004**, *108*, 5882.
[51] I. Pastoriza-Santos, D. Gómez, J. Pérez-Juste, L. M. Liz-Marzán, P. Mulvaney, *Phys. Chem. Chem. Phys.* **2004**, *6*, 5056.
[52] P. R. van Rheenen, M. J. McKelvy, W. S. Glausinger, *J. Solid State Chem.* **1987**, *67*, 151.

Received: June 19, 2006
Revised: September 6, 2006
Published online: October 20, 2006

